Biomass Conversion and Biorefinery
https://doi.org/10.1007/s13399-023-04542-w

ORIGINAL ARTICLE

Titanium dioxide nanoparticles: green synthesis, characterization, and antimicrobial/photocatalytic activity

Pâmela Cristine Ladwig Muraro[1] · Robson Dias Wouters[1] · Gabriela Pereira Chuy[1] · Bruno Stefanello Vizzotto[1] · Altevir Rossato Viana[1] · Giovani Pavoski[2] · Denise Crocce Romano Espinosa[2] · Virginia Cielo Rech[1] · William Leonardo da Silva[1]

Received: 18 April 2023 / Revised: 21 June 2023 / Accepted: 22 June 2023

Abstract
The work aims to biosynthesize and characterize titanium dioxide nanoparticles (TiO_2-NPs) to evaluate antimicrobial activity, cytotoxicity, and photocatalytic activity (under visible irradiation). X-ray diffraction (XRD), N_2 adsorption/desorption, zeta potential (ZP), field emission gun scanning electron microscopy (FEG-SEM), and scanning electron microscopy with energy-dispersive X-ray analysis (SEM–EDX) were used to characterize. The antibacterial potential was evaluated by minimal inhibitory activity (MIC) against *S. aureus* and *P. aeruginosa*. Central composite rotational design (CCRD 2^3) was used for experimental design. XRD diffractogram and FEG-SEM micrograph showed characteristic peaks of TiO_2-NPs (about 32 nm) and spherical shapes, respectively. TiO_2-NPs had a negative charge surface (−4.9 mV) with type V and H1 hysteresis and $S_{BET} = 118\ m^2\ g^{-1}$, Dp = 9.2 nm and Vp = 0.2 $cm^3\ g^{-1}$. EDX results indicated the presence of TiO_2-NPs and the effectiveness of the green synthesis. The antimicrobial activity showed that there was no inhibition of any pathogen. About the safety profile, there was no reduction in cell viability in the 293 T, MDBK, and HaCat cell lines, and reactive oxygen species (ROS) generation did not cause significant differences about the untreated control, indicating biocompatibility. The photocatalytic activity showed degradation of 90% of RhB dye using the ideal condition ([RhB] = 10 mg L^{-1}, [TiO_2-NPs] = 3.5 g L^{-1}, and pH = 7.0) by CCRD under visible irradiation with a pseudo-first-order kinetic model ($k = 0.0146\ min^{-1}$). Therefore, TiO_2-NPs present applications as alternative metallic nanoparticles for wastewater treatment and show potential for antimicrobial activity.

Keywords Titanium dioxide nanoparticles · Green synthesis · Heterogeneous photocatalysis · Wastewater treatment

1 Introduction

The growing concern with the pollution of the aquatic ecosystem makes it essential to develop ecologically appropriate and economically viable technologies for wastewater treatment, especially with emerging organic pollutants [1]. Dyes are chemical compounds that color materials and surfaces [2]. They are present in several industries, such as plastics, papers, leather, and textiles, to provide a specific coloring to the final product [3]. Among synthetic dyes, Rhodamine B (RhB) is an important laser dye with excellent photophysical properties such as long-wavelength absorption and emission, high fluorescence quantum yield, and large extinction coefficient, and it is classified as highly dangerous properties [4]. Colored wastewater is a major problem due to the diversity of compounds (with different functional groups) and the high biological stability of industrial dyes. Thus, conventional treatments such as physical–chemical present low removal for these organic pollutants [5]. Thus, it is necessary to use effective techniques to correct the treatment of dyes wastewater, such as the advanced oxidative processes (AOPs), including heterogeneous photocatalysis [6–8]. AOPs are based on the production of highly oxidizing radicals (•OH) under ultraviolet (UV) or visible irradiation, resulting mainly in the complete mineralization of

✉ William Leonardo da Silva
w.silva@ufn.edu.br

[1] Applied Nanomaterials Research Group (GPNAp), Nanoscience Graduate Program, Franciscan University, Santa Maria, RS, Brazil

[2] Polytechnical School of Chemical Engineering, University of the Sao Paulo, São Paulo, SP, Brazil

Published online: 01 July 2023

the persistent organic pollutants in CO_2, H_2O, and inorganic ions [9, 10].

Heterogeneous photocatalysis is a process that uses the semiconductor (denominated catalyst) induced under irradiation, promoting the hydroxyl radical generation by redox reaction [11]. Moreover, the high efficiency of heterogeneous photocatalysis is based on the redox reactions between the organic pollutant molecules adsorbed onto the catalytic surface and the hydroxyl radicals, avoiding possible recombination of the electron/hole pairs [12].

However, some semiconductors have specific limitations to the application under visible irradiation, such as titanium dioxide commercial [13], for example, due to the high band gap energy. Thus, it is necessary to research alternative and promising materials associated with nanotechnology, such as nanostructured systems [14, 15].

Nanostructured systems have specific textural, morphological, and structural properties that allow interactions with biomolecules, making them essential for applications at the biotechnological level, such as green metallic nanoparticles [16], and supported nanocatalysts for dye removal [17]. Green synthesis represents the processes between different metabolites or biomolecules, acting as reducing agents, with a primary precursor, being non-toxic, biodegradable, and low-biological [18, 19]. Among the eco-friendly metallic nanoparticles, TiO_2-NPs have been used in biomedical sciences [20], technological sciences [21], and agricultural sciences [22] due to the properties of non-toxicity, high specific surface area, and biocompatibility.

Thus, this work aims to biosynthesize and characterize titanium dioxide nanoparticles (TiO_2-NPs) from *Aloe vera* extract as a reducing agent and to evaluate the antimicrobial activity (*S. aureus* and *P. aeruginosa*), cytotoxicity (293 T, MDBK, and HaCat cell lines), and photocatalytic activity for the RhB dye removal under visible irradiation. The novelty of this works is the green synthesis of TiO_2-NPs with the presence of the photoactive phase (anatase), without the need for a heat treatment step. Furthermore, it demands the achievement of the Sustainable Development Goals (SDGs), specifically goals 6 (Potable water) and 14 (Life in water) correlating with topics of nanotechnology and toxicity.

2 Materials and methods

2.1 Aloe vera extract (AvE) and TiO_2-NP green synthesis

Aloe vera leaves (*Aloe arborescens*) were collected in Santa Maria (29° 41′ 29″ S, 53° 48′ 3″ W) and dried at 25 ± 2 °C for 24 h (Forced Air Lab Oven Cubic Foot 39.4 L) with a relative humidity of around 60% and a heating rate of 4 °C min^{-1}. After, the dry material was grounded in a knife mill (Willye TE-650) and sieved (#106 nm). Thus, 30 g of ground leaves were mixed with distilled water (30 min/250 rpm/25 ± 2 °C) [23]. TiO_2-NPs were synthesized by the green synthesis method [24]. For the bioreduction and nucleation steps, 130 mL of titanium isopropoxide (0.25 mol L^{-1}, $C_{12}H_{28}O4Ti$, Sigma-Aldrich®, 97%) and 150 mL of *AvE*t were mixed (90 min/250 rpm/25 ± 2 °C). After, for the stabilization step, TiO_2-NPs were dried (80 °C/720 min) (Fig. 1).

2.2 Characterization techniques

X-ray diffraction (XRD) was used to verify the TiO_2-NPs crystallinity or amorphism using a Bruker diffractometer (model D2 Advance) with $\lambda_{Cu\text{-}\alpha} = 0.15418$ nm ranging from 10°–70°, 30 kV (acceleration voltage) and 30 mA (applied current), where Debye–Scherer equation was used to determine the particle size of TiO_2-NPs, according to Eq. (1) [25]:

$$d = \frac{0.9\lambda}{\beta\cos(\theta)} \quad (1)$$

where $\lambda = 0.15418$ nm, β is the FWHM (full width at half maximum), and θ (°) is the Bragg diffraction angle.

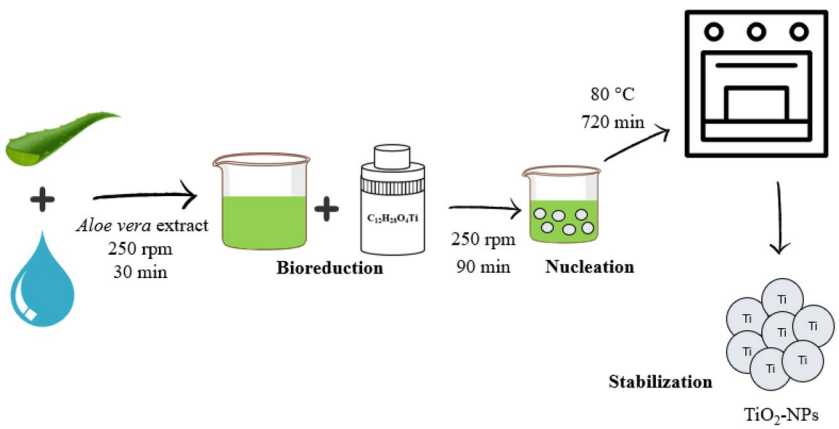

Fig. 1 Schematic representation of the TiO_2-NPs from AvE

Field emission gun scanning electron microscopy (FEG-SEM) was used to determine the morphological characteristic in a MIRA3 (TESCAN, Czech Republic) with 15 kV acceleration and 25 mm working distance with 400 and 5700 × magnification. The size of the TiO_2-NPs was measured using ImageJ software (NIH, USA), where 50 random points were selected and used to calculate the mean. Malvern-Zetasizer® model nanoZS (ZEN3600) was used to measure the surface charge value by zeta potential using closed capillary cells (DTS 1060). The specific surface area (S_{BET}) and pore size distribution (Vp and Dp) were determined in the ASAP 2020 Plus Micromeritics equipment using the BET/BJH method [26]. To identify the elements, energy-dispersive X-ray spectroscopy (EDX) was used in a Phenom Pro X microscope (Thermo Fisher Scientific) with 4000 × magnification at 15 kV and full backscattered electron. High performance liquid chromatography (HPLC) equipped with gradient elution capability, ultraviolet spectrophotometer and photodiode array as detector and an autosampler was used to the determination of *Aloe vera* extract composition. Data processing system used was the LabSolutions. A C18 reverse column (3.9 × 150 mm, 4 µL). Gradient elution consisted of two mobile phases (a) water (99.7%) and formic acid (0.3%) and (b) methanol (99.7%) and formic acid (0.03%). The detection wavelength was 280 nm and the flow rate was 1.0 mL min^{-1}. Each injection volume was 20 µL, and the column temperature was maintained at ambient conditions (25 ± 2 °C) [27].

2.3 Antimicrobial activity

MIC was carried out against *S. aureus* (ATCC 25923) and *P. aeruginosa* (ATCC 27853) by microdilution method [28] in triplicate with TiO_2-NP solution. one hundred microliters of Mueller Hinton broth (MH, Sigma-Aldrich®) was mixed with TiO_2-NPs (1:1 v/v), followed by a series of dilutions (500–0.98 µg mL^{-1}). Bacterial inoculum (1×10^8 CFU mL^{-1}) was added and incubated (24 h/37 ± 2 °C). After, TTC (5% w/w) was added and reincubated (2 h/37 ± 2 °C). MHB only was used as negative control and MHB with bacterial inoculum was used as positive control.

2.4 Cell cultivation

293 T (embryonic kidney human, ATCC CRL-3216), MDBK (kidney bovine, ATCC CCL-22), and HaCat (human keratinocyte, ATCC PCS-200-011TN™) cell lines from the Cell Bank (Rio de Janeiro, Brazil) were used to determine the safety profile of the TiO_2-NPs. Cells were cultured using Dulbecco's modified Eagle medium (DMEM, Sigma-Aldrich®) with 10% fetal bovine serum (FBS) (Sigma-Aldrich®) and 1% penicillin–streptomycin-neomycin (PSN) antibiotic mixture [29]. Cells were kept in a 5% CO_2 incubator at 37 ± 2 °C with controlled humidity. These cells were seeded in 96-well plates (1–300 µg mL^{-1}) during 24 h of incubation. One hundred millimoles per liter of hydrogen peroxide (H_2O_2) was used as a positive control (PC) for cell viability and ROS generations, while for the NO generation sodium nitrite ($NaNO_2$, 1 µg mL^{-1}) was used. Negative control (NC) was the cells in the culture.

2.5 Cell viability

To determine the cell viability (24 h) was carried out the 3-(4,5-dimethylthiazol-2-yl)-2,5-diphenyl tetrazolium bromide MTT test [30,31]. Thus, 20 µL of the TiO_2-NPs was mixed with MTT solution MTT (5 mg mL^{-1}) and incubated (4 h/37 ± 2 °C/5% CO_2). The solution was carefully removed and the formazan crystals dissolved in 200 µL of the DMSO. Cell growth inhibition was detected using a microplate reader (Biochrom® Anthos) at λ = 570 nm.

2.6 Semi-quantification of reactive oxygen species (ROS)

ROS generation was determined by the DCFH- DA (2,7-dichlorofluorescein diacetate) [32] with TiO_2-NPs extracts (1–300 µg mL^{-1}). DCFH-DA solution (1 mmol L^{-1}) was diluted in ethanol (1:10 v/v). Ten microliters of the solution was mixed with Tris HCl (65 µL) and treated cells (50 µL). After, the solution was incubated (1 h/37 ± 2 °C/5% CO_2), and the fluorescence intensity was determined at 520 nm of emission and 480 nm of excitation using a microplate reader (Biochrom® Anthos).

2.7 Indirect determination of nitric oxide generation

Griess solution (0.1% N-(1-naphthyl)ethylenediamine dihydrochloride, and 1% sulfanilamide in 5% phosphoric acid) was used to detect the presence of nitrites (NO_2^-) in the sample, which is a NO metabolite, according to the literature [33]. Thus, 100 µL of the TiO_2-NP extracts (1–300 µg mL^{-1}) was added to a 96-well plate with Griess solution (100 µL) and incubated (30 min/37 ± 2 °C/5% CO_2). After, an ELISA reader (photometer) was used to determine the intensity of the formed color (λ = 540 nm).

2.8 Photocatalytic activity

RhB dye was used as the target molecule in contact with TiO_2-NPs for 60 min (without radiation) and 180 min under visible irradiation, where aliquots were collected at predetermined times (0, 5, 15, 30, 45, 60, 75, 90, 120, 150, and 180 min). All samples were filtered (ϕ = 0.45 µm) and

diluted (1:10 v/v). To determine the photodegradation (%R) of RhB dye, a UV–vis spectrophotometer (Varian Cary 100) was used at λ = 553 nm.

2.9 Photodegradation kinetic

The Langmuir–Hinshelwood model (L–H) was used for the kinetic study of experimental data, according to Eqs. (2) and (3) [34, 35]:

$$(-r_i) = -\frac{dC_i}{dt} = \frac{k_s.K.C_i}{1 + K.C_i} \quad (2)$$

$$C_i = C_{io}.e^{-k.t} \quad (3)$$

where $(-r_i)$ is the reaction rate (mol·min^{-1}·L^{-1}), K is the adsorption constant, k_s is the apparent constant of reaction, C_{io} is the initial RhB dye concentration, C_i is the RhB dye concentration, and k is the apparent rate of the pseudo-first-order reaction (min^{-1}).

2.9.1 CCRD

CCRD 2^3 was used to determine the ideal condition of the heterogeneous photocatalysis process using pH, RhB concentration (mg L^{-1}), and TiO_2-NPs concentration (g L^{-1}) as independent variables, and as the response variable, the percentage of photodegradation (Table 1).

2.10 TiO_2-NPs recycling

After the first cycle, the RhB solution was centrifuged (5000 rpm/10 min), and TiO_2-NPs were separated and reintroduced into the reactor using the ideal condition by CCRD. Therefore, the procedure was repeated five times, and the percentage of the degradation and the apparent rate of the pseudo-first-order reaction were calculated.

2.11 Statistic analysis

To determine the ideal condition, the Statistical 10 software (StatSof, Tulsa, USA) was used through surface response analysis and ANOVA ($p < 0.05$). GraphPad Prism and Tukey's post hoc test were used for all the biological tests with $*p < 0.05$, $**p < 0.01$, and $***p < 0.001$.

Table 1 CCRD 2^3 experimental design for the photocatalytic tests

Order	[RhB]	[TiO_2-NPs]	pH
(− 1.68)	1.6	1.0	2.0
(− 1)	5	2.0	4.0
0	10	3.5	7.0
(+ 1)	15	5.0	10.0
(+ 1.68)	18.4	6.0	12.0

3 Results and discussion

3.1 Characterization of the AvE and TiO_2-NPs

Table 2 shows the AvE chromatogram by HPLC, where it was possible to detect a series of bioactive compounds such as the following: (a) phenolic compounds—ellagic acid, epigallocatechin gallate, and catechin in the concentration of 99.79, 0.16, and 38.80 mg L^{-1}, respectively; (b) flavonoids—naringin, myricetin, quercetin, and kaempferol in the concentration of 97.39, 103.05, 1.96, and 108.29 mg L^{-1}, respectively. The identified compounds play different roles in preventing and treating pathologies [36]. It is noteworthy that the presence of these functional biomolecules from *Aloe vera* extract is responsible for the active reduction step of metal ions ($Ti^{+4} \rightarrow Ti^0$), due to the presence of a series of functional groups (e.g., –C–O–C, – C–O–, –C = C–, and –C = O–), derived from heterocyclic compounds. Then, the metal ions aggregate and form metal nanoparticles (nucleation step), where the biocompounds form a stabilizing layer around the nanoparticles, preventing them from aggregating [37, 38].

Figure 2 shows the XRD diffraction with characteristic peaks at 25.20° (101), 37.71° (004), 47.89° (200), 53.71° (105), 54.98° (211), and 62.58° (204) with a = 3.755 Å and c = 9.5114 Å, confirming the anatase phase of TiO_2-NPs according to the JCPDS file 21–1272 31 [39] and 32 nm of the particle size. In addition, the peak at 36.0º (101) was assigned to the rutile phase [40]. Among the polymorphic phases of TiO_2-NPs, the most active phase photocatalytic is anatase, with a high surface area, slower recombination, and greater electron mobility [41], indicating that it was possible to synthesize a titanium dioxide nanostructured

Table 2 Metabolite identification by HPLC from AvE

Component	RT (min)	Area	Area %	Concentration (mg L^{-1})
Gallic acid	1.04	12,641	0.124	0.56
Catechin	1.63	878,542	8.6205	38.80
Epigallocatechin gallate	2.08	3653	0.0358	0.16
Ellagic acid	7.11	2,259,891	22.1747	99.79
Naringin	8.91	2,205,661	21.6426	97.39
Myricetin	10.72	2,333,897	22.9009	103.05
Quercetin	11.17	44,466	0.4363	1.96
Kaempeferol	12.57	2,452,542	24.0652	108.29

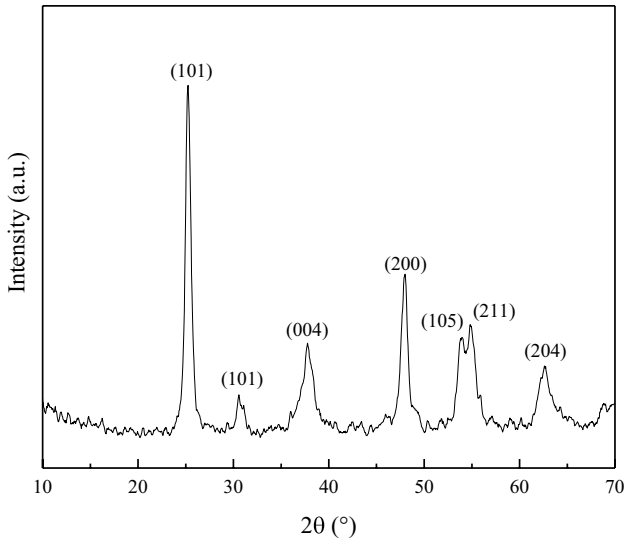

Fig. 2 XRD diffractogram of the TiO_2-NPs from AvE

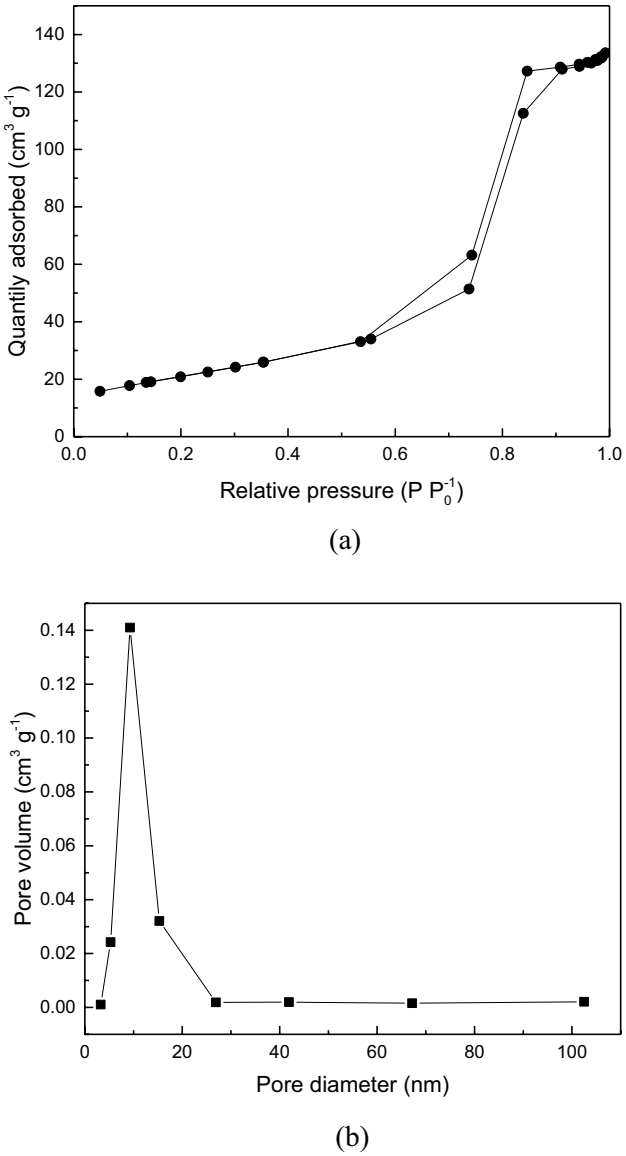

Fig. 3 **a** N_2 adsorption/desorption isotherm and **b** the distribution of the pore volume of the TiO_2-NPs from AvE

with the predominance of the active phase, without the need for thermal treatment.

About the textural and structural properties, TiO_2-NPs showed S_{BET} of 118 m^2 g^{-1}, Dp of 9.2 nm, and Vp of the 0.2 cm^3 g^{-1}, indicating a mesoporous characteristic, high specific surface area, and considerable porosity [42, 43], and a negative charge surface (-4.90 ± 0.30 mV) compatible with RhB cationic dye.

Figure 3a shows the adsorption/desorption isotherm of the TiO_2-NPs, which was characterized for type V with H1 hysteresis (uniform spheres with a form of cylinders and open ends) [44, 45], while the Fig. 3b illustrates the pore size distribution curve.

Figure 4a shows the FEG-SEM micrographs where it was possible to visualize a heterogeneous surface with small agglomerations of TiO_2-NPs and irregular particle sizes, which indicates an interconnection between the pores [46] with a particle diameter around 287 ± 115 nm (Fig. 4b). Moreover, it is possible to verify a spherical morphology of the nanoparticles with considerable porosity, favoring the interparticle diffusion of RhB molecules into the active site, increasing the amount of hydroxyl radical generated and directly affecting the photocatalytic activity [47].

To investigate the elemental composition of the TiO_2-NPs, SEM–EDX was carried out according to Fig. 5, where there was a predominance of oxygen (62.42%) and titanium (30.63%), resulting in the formation of titanium dioxide nanoparticles from the reduction metallic precursor (Ti^{+4}), with a heterogeneous morphology of approximately small nanocrystals, giving a large surface area and promoting the formation of clusters [48].

3.2 Antimicrobial activity

The antibacterial potential was evaluated by MIC assay, indicating that there was no antimicrobial activity against the two pathogens respectively. TiO_2-NPs have greater antimicrobial activity depending on their particle size, and the smaller the diameter of the nanomaterial, the greater the toxicity when exposed to microorganisms [49–51]. Moreover, the decomposition of the bacterial outer membrane by reactive oxygen species (ROS) is a bactericidal effect attributed to the TiO_2-NPs [52, 53]. Thus, the textural properties of TiO_2-NPs (S_{BET}, Dp, and Vp), and the photoactive phase TiO_2-NPs did not allow efficient

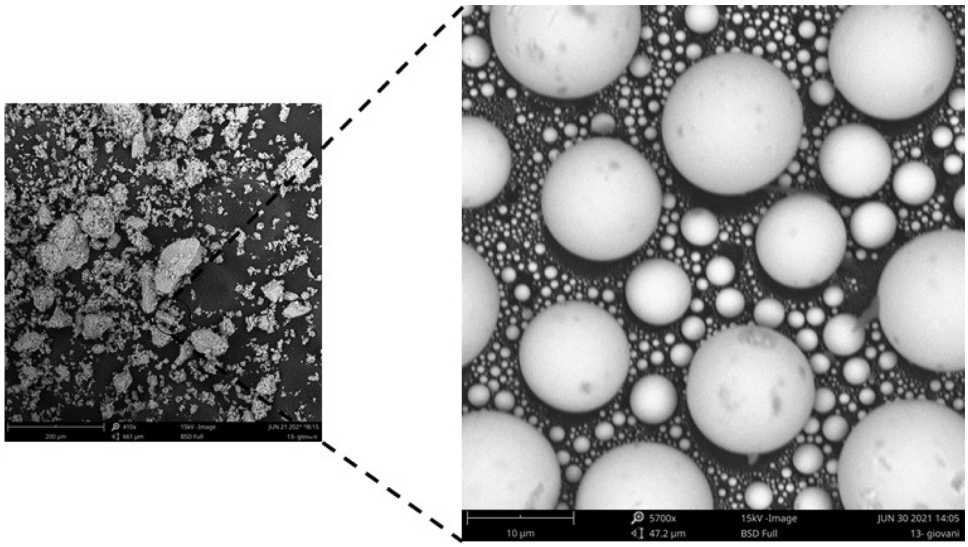

(a)

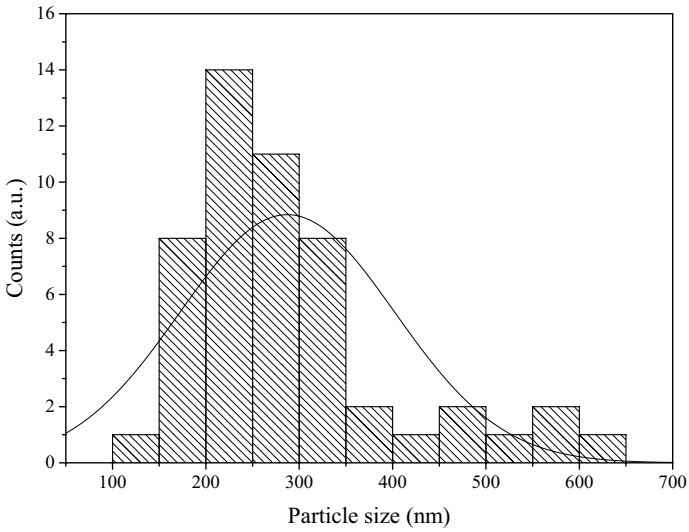

(b)

Fig. 4 **a** FEG-SEM micrograph and **b** average particle size of the TiO_2-NPs from AvE

contact with bacterial cells, limiting ROS generation, and the restricting mechanical resistance of the cell wall [54].

3.3 Cytotoxicity tests

Figure 6 shows the evaluation of cytotoxicity by the MMT test after 24 h, where it was possible to verify that in none of the treatments with TiO_2-NPs, there was a significant decrease in cell viability, only in the positive control.

According to Fig. 6, TiO_2-NP concentrations tested showed no significant decrease in cell viability, without toxicity and restricted proliferation, evidencing biocompatibility, and the possibility of expanding the application spectrum, as in biomaterials [55, 56]. Moreover, it is highlighted that TiO_2-NP toxicity depends in concentration, exposure time, and degree of tolerance of the cell line tested [57]. Positive control helps to show that negative (untreated) samples are negative. The results of the controls must be different to validate the test. A positive control usually uses a substance that the test reagent will detect.

3.4 ROS generation

Figure 7 represents the evaluation of the ROS generation after 24 h, where all tested concentrations of TiO_2-NPs did not produce the formation of free radical, except for the positive control, which significantly increased levels when compared to the NC.

According to Fig. 7, it was possible to notice that TiO_2-NPs did not cause an increase in ROS generation,

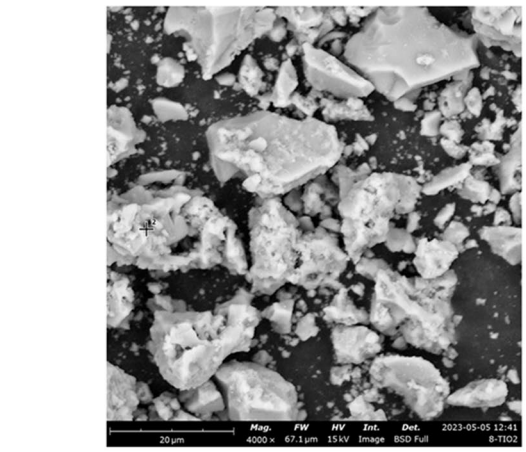

(a)

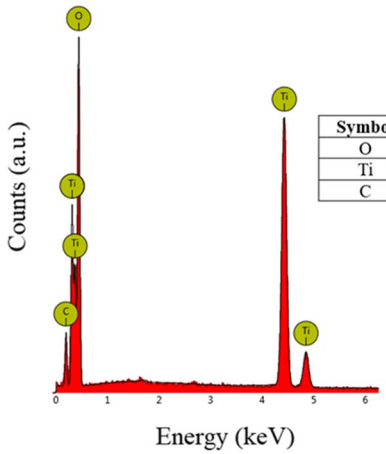

Symbol	Element	Weight (%)
O	Oxygen	62.42
Ti	Titanium	30.63
C	Carbon	6.95

(b)

Fig. 5 **a** SEM micrography with 4000× magnification and **b** EDX results of the TiO_2-NPs from AvE

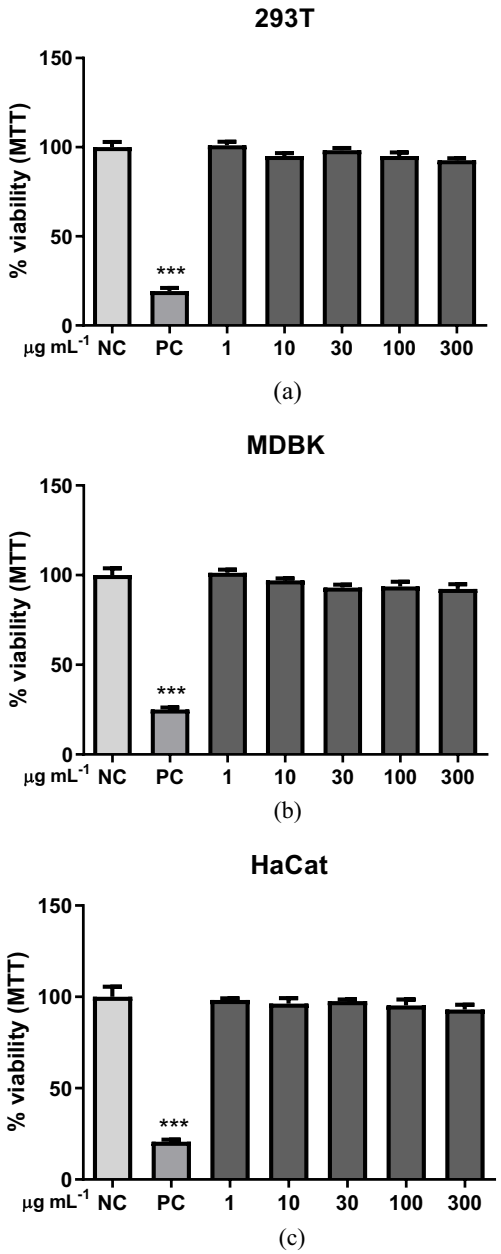

Fig. 6 Evaluation of cytotoxicity by the MTT test after 24 h. Data were presented as mean $*p<0.05$, $**p<0.01$, and $***p<0.001$ versus negative control (NC)

indicating that the green synthesis contributed to the production of nanoparticles free of chemical impurities, decreasing the ROS levels and being accepted in the medical field [58–60]. Moreover, the ROS generation using the TiO_2- NPs occurs when the particle is subjected to UV irradiation. Due to the wider band gap, there is absorption and production of reactive species [61] which was not the focus of the study, since visible radiation was used.

Initially, the oxidation of H2DCF to DCF was thought to be specific for H_2O_2. However, recent evidence, has shown that other ROS, such as hydroxyl radicals, hydroperoxides, and peroxynitrite can oxidize H2DCF but are much less sensitive than H_2O_2 [62]. However, the most used assay in cells is H_2O_2 [63].

3.5 NO generation

Figure 8 shows the evaluation of nitric oxide generation after 24 h, where it was impossible to detect nitrite in the supernatants treated with TiO_2-NPs.

According to Fig. 8, TiO_2-NP treatments showed no changes in NO levels, due to the green synthesis process used from extracts acting as reducing agents and the presence of the richness of biomolecules [64, 65]. In the NO test, NO and its by-products, such as NO_3^- and NO_2^-, can

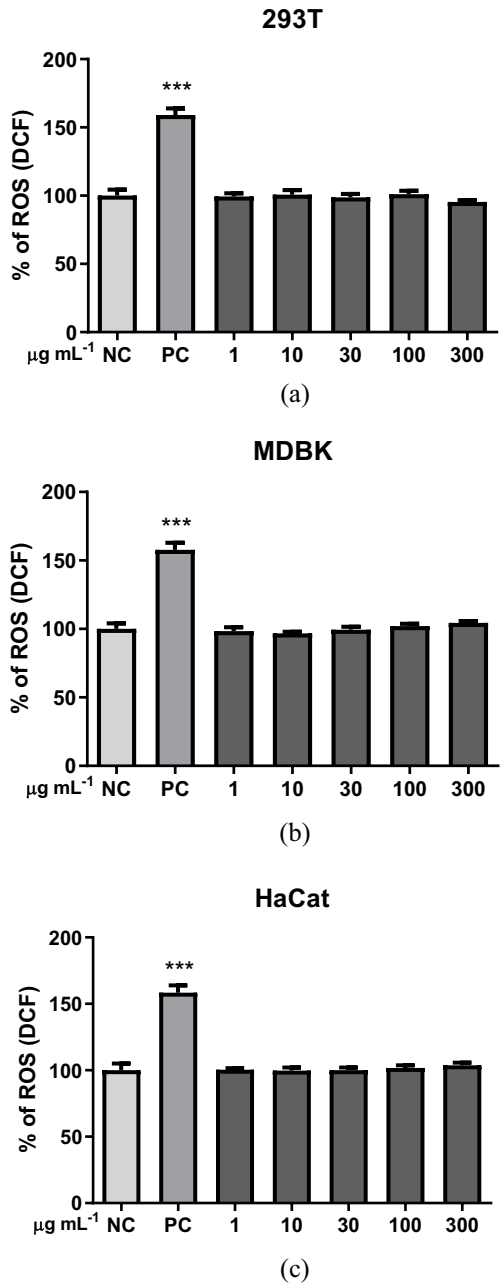

Fig. 7 Evaluation of ROS generation after 24 h. Data were presented as mean $*p<0.05$, $**p<0.01$, and $***p<0.001$ versus negative control (NC)

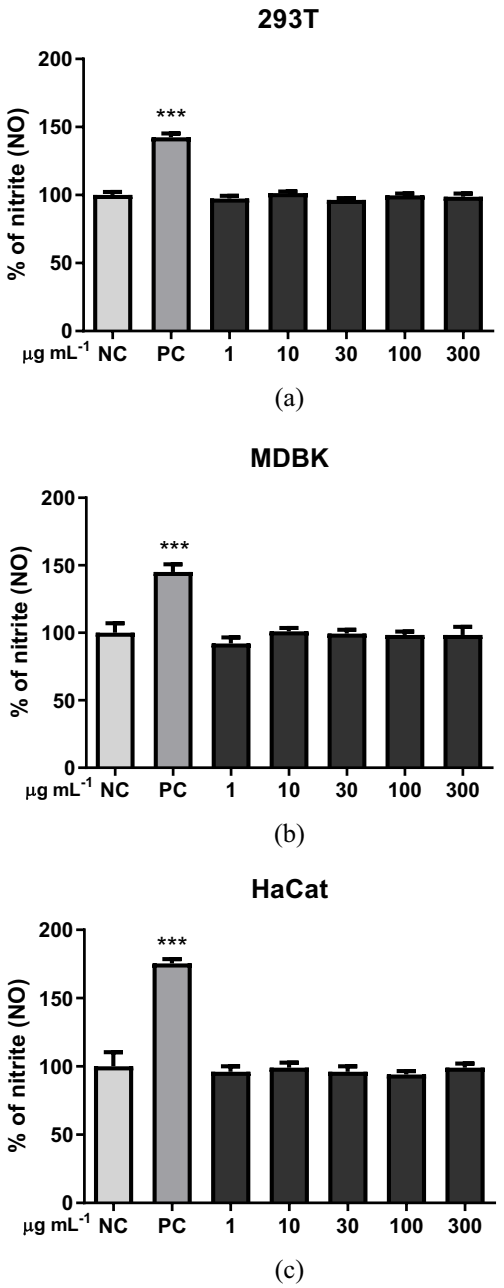

Fig. 8 Evaluation of NO generation after 24 h. Data were presented as mean $*p<0.05$, $**p<0.01$, and $***p<0.001$ versus negative control (NC). *NC: cells in culture medium; PC: 1 µg mL^{-1} of the $NaNO_2$ and treatments (1; 10; 30, 100, and 300 µg $mL.^{-1}$ of TiO_2-NPs)

be measured indirectly [66]. Sodium nitrite is often used with the Griess reagent to generate a standard curve [67] because low concentrations (0.1 µg mL^{-1}) can be detected using this method [68].

3.6 CCRD

Figure 9 shows the Pareto graphic where it was possible to verify that the pH and [TiO_2-NPs] showed a quadratic indirect effect on the percentage of RhB dye removal, because of the reduction in the number of active sites available for intermolecular diffusion of RhB molecules [69]. However, a high concentration of TiO_2-NPs will decrease the degradation percentage, as visible radiation penetration into the aqueous medium will be reduced, making it an opaque system [70]. Regarding the pH effect,

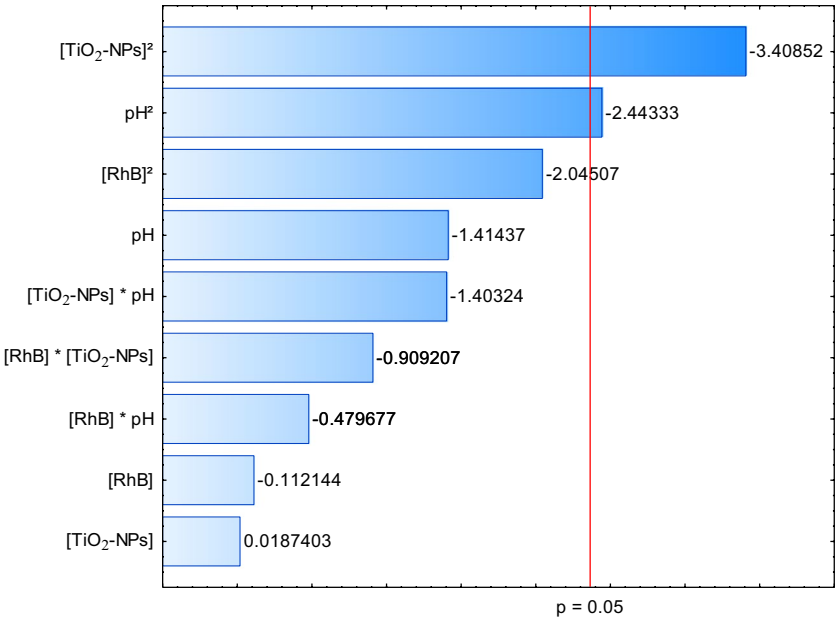

Fig. 9 Pareto chart using input variables and output parameters under visible radiation

when the pH variation in higher or lower values provides the formation of the nanoparticles negative or positive surface charges, affecting the adsorption–desorption of the RhB molecules [71]. For acidic pH, low dye degradation using the TiO_2-NPs was observed, due to the low electrostatic attraction, due to the repulsion between the target molecule and catalytic surface. However, the hydroxyl radicals are slowly absorbed, not having a high reaction with the dye under basic pH [72], favoring neutral pH for the reaction. Equation (4) shows the %R of the RhB depending on the pH and [TiO_2-NPs], and Fig. 10 demonstrates the 3D surface response, indicating the ideal condition was [RhB] = 10 mg L^{-1}, [TiO_2-NPs] = 3.5 g L^{-1}, and pH = 7.0 at 25 ± 2 °C, which showed the greatest degradation of 90% after 180 min under visible radiation.

$$\%R = 234.74 - 9.12xpH^2 - 1.63x[TiO_2 - NPs]^2 \quad (4)$$

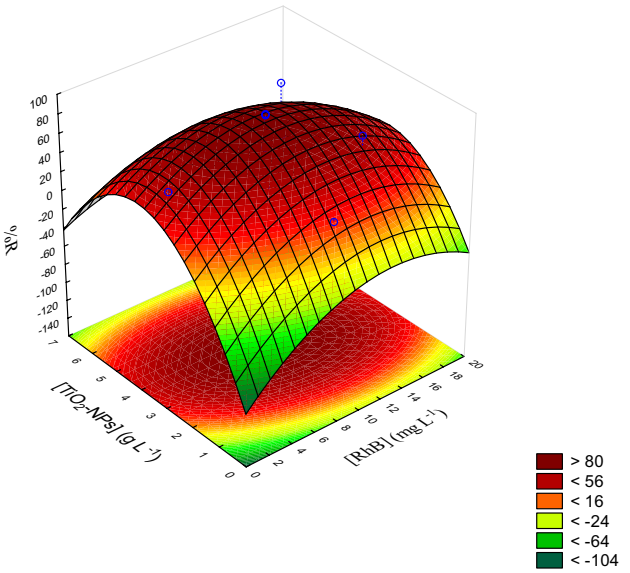

Fig. 10 3D surface response for RhB photodegradation under visible radiation

3.7 Photocatalytic activity and recycling

Figure 11 shows the photocatalytic activity of TiO_2-NPs under visible radiation using the ideal condition ([RhB] = 10 mg L^{-1}, [TiO_2-NPs] = 3.5 g L^{-1} and pH = 7.0) after 180 min with 90% degradation. Moreover, it was possible to verify a pseudo-first-order kinetic model with an apparent rate of the pseudo-first-order reaction specific reaction (k) of 0.0146 min^{-1}, according to the literature [73, 74].

Figure 12 shows the TiO_2-NPs recycling after five cycles with a decrease in RhB degradation (90 to 84.67%) and a decrease in the specific reaction rate (k) for k = 0.0146 min^{-1} for 0.0125 min^{-1}, indicating the stability of the nanocatalyst.

The general mechanism for heterogeneous photocatalysis using TiO_2-NPs as a nanocatalyst has the following steps [75] (Fig. 13): (a) adsorption of RhB molecules onto the TiO_2-NPs (Eq. 5); (b) excitation of the TiO_2-NPs (Eq. 6); (c) load recombination (Eq. 7); (d) singlet oxygen formation (Eq. 8); (e) production of $^{\bullet}OH$ radicals from O_2 (Eq. 9), and (f) RhB degradation (Eq. 10). Thus, the efficiency of the

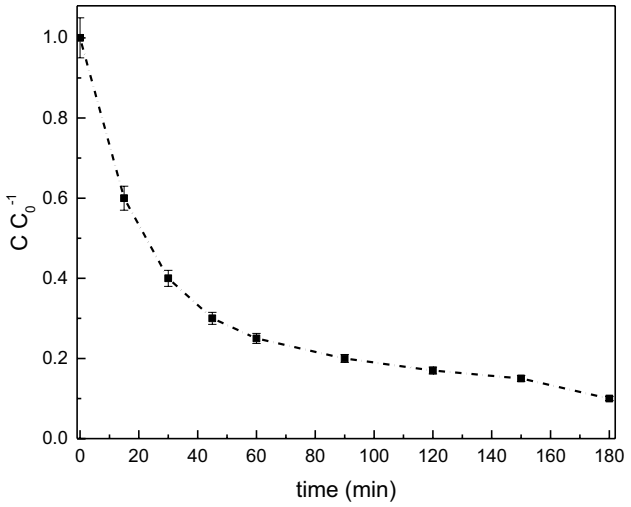

Fig. 11 Photocatalytic activity of the TiO_2-NPs under visible radiation

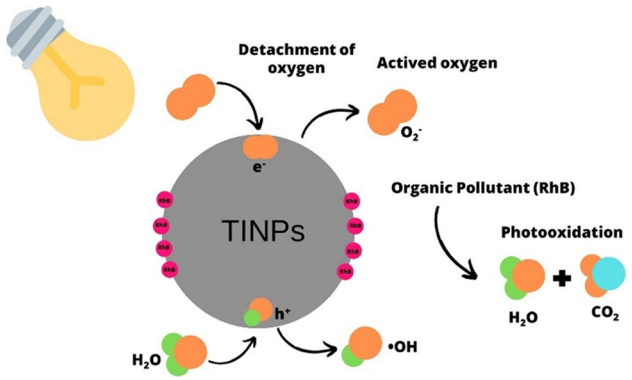

Fig. 13 Mechanism of RhB degradation by the photocatalysis process

photocatalytic process depends directly on the competition between electrons removed from the semiconductor surface and on the possible recombination of electron/vacancy pairs.

$$TiO_2 - NPs^{+}\left(O_2 + H_2O + RhB\right) \rightarrow O_{2(Ads)} + H_2O_{(Ads)}RhB_{(Ads)} \quad (5)$$

$$TiO_2 - NPs + h\nu \rightarrow e^{-}{}_{CB} + h^{+}{}_{VB} \quad (6)$$

$$e^{-}{}_{CB} + h^{+}{}_{VB} \rightarrow \text{Heatliberation} \quad (7)$$

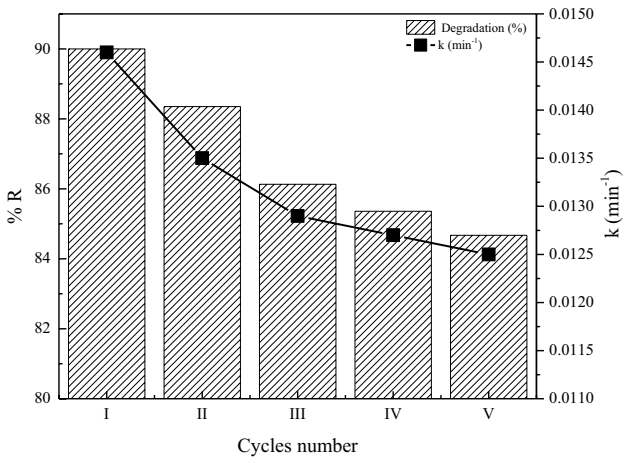

Fig. 12 Effect of the TiO_2-NPs recycling for RhB degradation

$$O_{2(Ads)} + e^{-}{}_{CB} \rightarrow O_2{}^{\cdot -} \quad (8)$$

$$H_2O_2 + O_2{}^{\cdot -} \rightarrow O_2 + {}^{\cdot}OH \quad (9)$$

$$Rhb + {}^{\cdot}OH \rightarrow products\left(CO_2 + H_2O\right) \quad (10)$$

Different metallic nanoparticles have been reported in the literature to remove RhB dye using heterogeneous photocatalysts such as Ag@ZnO, TiO_2@HNTs, AgNPs@BC, Fe@Bi-P-I, and AgBr@SnO_2, indicating a versatility for the use of commercial semiconductors. However, aiming for sustainable development and green technology, it is necessary to search for new nanocatalysts from extracts or residual biomass using the green synthesis process, such as metallic nanoparticles. Thus, Table 3 shows some studies about RhB degradation using different nanocatalysts.

According to Table 3, green synthesis has already been consolidated to obtain metallic nanoparticles. Thus, the advantages of this synthesis process compared to traditional processes (e.g., hydrothermal, coprecipitation, sol–gel) is its versatility and the easy access of biomolecules present in plant extracts to act as bioreducing agents, not requiring toxic reagents, meeting sustainable development.

4 Conclusion

TiO_2-NPs were prepared from *Aloe vera* extract using the green synthesis process for application in the RhB removal by the heterogeneous photocatalysis process. The N_2 porosimetry showed $S_{BET} = 118\ m^2\ g^{-1}$, $Vp = 0.2\ cm^3\ g^{-1}$, and $Dp = 9.2$ nm, indicating a nanometric structure of the material with mesoporous characteristics and

Table 3 Comparative studies for RhB removal by of heterogeneous photocatalysis with metallic nanoparticles

Nanocatalyst	Comment	[Catalyst] (g L^{-1})	[RhB] mg L^{-1})	pH	Degradation (%)	Reference
Ag@ZnO	Synthesis of silver-doped zinc oxide nanoparticles for photocatalytic degradation of RhB under sunlight radiation	0.05	20	-	85.52	[76]
TiO_2@HNTs	Synthesis of TiO_2@HNTs for RhB degradation under UV radiation	0.4	20	-	96.84	[77]
AgNPs@BC	Biosynthesis of AgNPs@BC nanoparticles for photocatalytic degradation of RhB under visible radiation	2.0	50	9.3	99.9	[78]
Fe@Bi-P-I	Fe/Bi-P-I synthesis for photocatalytic degradation of RhB under sunlight radiation	0.6	10	10	99.58	[79]
AgBr@SnO_2	Synthesis of AgBr/SnO_2 for photocatalytic degradation of RhB under UV and visible radiation	1	10	5.5	95 and 85	[80]
TiO_2-NPs	TiO_2-NP green synthesis for photocatalytic degradation of RhB under visible radiation	3.5	10	7.0	90	In this study

considerable porosity. XRD diffractogram showed characteristic peaks of the anatase active phase and d = 32 nm. FEG-SEM micrographs indicated a morphology of the nanoparticles with small clusters (about 32 cm) and a spherical structure. Furthermore, the zeta potential indicated a negative surface charge of − 4.90 mV, favoring the electrostatic interaction with the target molecule (RhB-cationic dye). The antimicrobial activity showed that the TiO_2-NPs had no effective activity against the tested pathogens. About the heterogeneous photocatalysis process, when exposed to TiO_2-NPs under visible radiation, 90% degradation was observed using the ideal conditions (pH = 10; [TiO_2-NPs] = 3.5 g L^{-1}; [RhB] = 10 mg L^{-1}). The kinetic study indicated pseudo-first-order behavior with $k = 0.0146$ min^{-1}. Regarding the in vitro safety of TiO_2-NPs, there was no reduction in cell viability in the 293 T, MDBK, and HaCat cell lines. In the ROS generation, the concentrations (1–300 µg mL^{-1}) used did not cause significant differences from the untreated control, showing that there is preliminary biocompatibility. Therefore, TiO_2-NPs have potential application as nanocatalysts for the degradation of dye wastewater by the heterogeneous photocatalysis process.

Acknowledgements USP (LAREX, Brazil – SP) and UFN (Brazil – RS) for the support.

Author contribution Muraro, P.C.L.: conceptualization, data curation, formal analysis, investigation, validation, writing—original draft, writing—review, and editing. Wouters, R. D.: conceptualization, writing—review, and editing. Chuy, G.: antimicrobial test, writing—review, and editing. Vizzotto, B.S.: conceptualization, validation, writing—review and editing. Viana, A.R.: MTT, DCFH-DA, and NO test, writing—review, and editing. Pavoski, G.: conceptualization, data curation, formal analysis, and editing. Espinosa, D.C.R.: conceptualization, writing—review, and editing. Rech, V.C.: conceptualization, validation, writing—review, and editing. Da Silva, W.L.: conceptualization, data curation, formal analysis, investigation, validation, writing—original draft, writing—review and editing.

Funding This study was financed in part by the Coordenação de Aperfeiçoamento de Pessoal de Nível Superior—Brasil (CAPES)—Finance Code 001.

Data availability The data that support the findings of this study are available on request from the corresponding author.

Declarations

Competing interests The authors declare no competing interests.

References

1. Arruda TLD, Jardim WF (2007) Treatment of groundwater contaminated with chlorinated compounds using elemental iron and Fenton's reagent. Quim Nova 30:1628–1632. https://doi.org/10.1590/S0100-40422007000700024
2. Singh S, Parveen N, Gupta H (2018) Adsorptive decontamination of rhodamine-B from water using banana peel powder: a biosorbent. Environ Technol Innov 12:189–195. https://doi.org/10.1016/j.eti.2018.09.001
3. Santhi M, Kumar PE (2015) Adsorption of Rhodamine B from an aqueous solution: kinetic, equilibrium and thermodynamic studies. Adsorption 4:497–510. https://doi.org/10.15680/IJIRSET.2015.0402039
4. Farag AAM, Yahia IS (2011) Rectification and barrier height inhomogeneous in Rhodamine B-based organic Schottky diode. Synth Met 161:32–39. https://doi.org/10.1016/j.synthmet.2010.10.030
5. Kanchana A, Devarajan S, Ayyappan SR (2010) Green synthesis and characterization of palladium nanoparticles and its conjugates from solanum trilobatum leaf extract. Nano-Micro Lett 2:169–176. https://doi.org/10.5101/nml.v2i3.p169-176

6. Lee K, Lai CW, Ngai KS, Juan JC (2016) Recent developments of zinc oxide based photocatalyst in water treatment technology: a review. Water Res 88:428–448. https://doi.org/10.1016/j.watres.2015.09.045
7. Ong C, Ng L, Mohammad A (2018) A review of ZnO nanoparticles as solar photocatalysts: Synthesis, mechanisms, and applications. Renew Sust Energy Rev 81:536–551. https://doi.org/10.1016/j.rser.2017.08.020
8. Ali W, Ullah H, Zada A, Alamgir MK, Muhammad KW, Ahmad MJ, Nadhman A (2018) Effect of calcination temperature on the photoactivity of ZnO/SnO2 nanocomposites for the degradation of methyl orange. Mater Chem Phys 213:259–266. https://doi.org/10.1016/j.matchemphys.2018.04.015
9. Miklos DB, Remy C, Jekel M, Linden KG, Drewes JE, Hübner U (2018) Evaluation of advanced oxidation processes for water and wastewater treatment–a critical review. Water Res 139:118–131. https://doi.org/10.1016/j.watres.2018.03.042
10. Brito GSF, Oliveira R, Grisolia CK, Guirra LS, Weber IT, Almeida FV (2019) Evaluation of advanced oxidative processes in biodiesel wastewater treatment. J Photochem Photobiol A: Chem 375:85–90. https://doi.org/10.1016/j.jphotochem.2019.01.013
11. Isari AA, Payan A, Fattahi M, Jorfi S, Kakavandi B (2018) Photocatalytic degradation of rhodamine B and real textile wastewater using Fe-doped TiO2 anchored on reduced graphene oxide (Fe-TiO2/rGO): Characterization and feasibility, mechanism and pathway studies. Appl Surf Sci 462:549–564. https://doi.org/10.1016/j.apsusc.2018.08.133
12. Pascoal SA, Lima CAPD, Sousa JTD, Lima GGCD, Vieira FF (2007) Application of artificial and solar UV radiation in the photocatalytic treatment of tannery effluents. Quim Nova 30:1082–1087. https://doi.org/10.1590/S0100-40422007000500006
13. Feltrin J, Sartor MN, Bernardin AM, Hotza D, Labrincha JÁ (2013) Photocatalytic surfaces of titania on ceramic substrates: part I: synthesis, structure, and photoactivity. Ceramica 59:620–632. https://doi.org/10.1590/S0366-69132013000400020
14. Wani WA, Prashar S, Shreaz S, Gomez-Ruiz S (2016) Nanostructured materials functionalized with metal complexes: In search of alternatives for administering anticancer metallodrugs. Coord Chem Rev 312:67–98. https://doi.org/10.1016/j.ccr.2016.01.001
15. Mauter MS, Zucker I, Perreault F, Werber JR, Kim JH, Elimelech M (2018) The role of nanotechnology in tackling global water challenges. Nat Sustain 1:166–175. https://doi.org/10.1038/s41893-018-0046-8
16. Barrientos Á, De La Fuente JM, Rojas TC, Fernández A, Penadés S (2003) Gold glyconanoparticles: synthetic polyvalent ligands mimicking glycocalyx-like surfaces as tools for glycobiological studies. Chem Eur J 9:1909–1921. https://doi.org/10.1002/chem.200204544
17. Oviedo L, Muraro PCL, Pavoski G, Espinosa DCR, Ruiz YPM, Galembeck A, Rhoden CB, Da Silva WL (2021) Synthesis and characterization of nanozeolite from (agro)industrial waste for application in heterogeneous photocatalysis. Environ Sci Pollut Res 29:3794–3807. https://doi.org/10.1007/s11356-021-15815-0
18. Mittal AK, Chisti Y, Banerjee UC (2013) Synthesis of metallic nanoparticles using plant extracts. Biotechnol Adv 31:346–356. https://doi.org/10.1016/j.biotechadv.2013.01.003
19. Faramarzi MA, Sadighi A (2013) Insights into biogenic and chemical production of inorganic nanomaterials and nanostructures. Adv Colloid Interface Sci 189:1–20. https://doi.org/10.1016/j.cis.2012.12.001
20. Gerhardt L, Jell G, Boccaccini A (2007) Titanium dioxide (TiO2) nanoparticles filled poly (D, L lactic acid) (PDLLA) matrix composites for bone tissue engineering. J Mater Sci: Mater Med 18:1287–1298. https://doi.org/10.1007/s10856-006-0062-5
21. Muraro PCL, Mortari SR, Vizzotto BS, Chuy G, Dos Santos C, Brum LFW, Da Silva WL (2020) Iron oxide nanocatalyst with titanium and silver nanoparticles: Synthesis, characterization and photocatalytic activity on the degradation of Rhodamine B dye. Sci Rep 10:3055–3063. https://doi.org/10.1038/s41598-020-59987-0
22. Rodríguez-González V, Terashima C, Fujishima A (2019) Applications of photocatalytic titanium dioxide-based nanomaterials in sustainable agriculture. J Photochem Photobiol C: Photochem Rev 40:49–67. https://doi.org/10.1016/j.jphotochemrev.2019.06.001
23. Chandran SP, Chaudhary M, Pasricha R, Ahmad A, Sastry M (2006) Synthesis of gold nanotriangles and silver nanoparticles using Aloe vera plant extract. Biotechn Progress 22:577–583. https://doi.org/10.1021/bp0501423
24. Wouters RD, Muraro PCL, Druzian DM, Viana AR, Pinto EO, Da Silva JKL, Vizzotto BS, Ruiz YPM, Galembeck A, Pavoski G, Espinosa DCR, Da Silva WL (2023) Zinc oxide nanoparticles: Biosynthesis, characterization, biological activity and photocatalytic degradation for tartrazine yellow dye. J Mol Liq 371:121090–121100. https://doi.org/10.1016/j.molliq.2022.121090
25. Cullit BD (1956) Elements of X-ray diffraction. Addison-Wesley Publishing Inc, United States
26. Thommes M, Kaneko K, Neimark AV, Olivier AP, Rodriguez-Reinoso F, Rouquerol J, Sing KSW (2015) Physisorption of gases, with special reference to the evaluation of surface area and pore size distribution (IUPAC Technical Report). Pure Appl Chem 87:1051–1069. https://doi.org/10.1515/pac-2014-1117
27. Matsubara S, Amaya DBR (2006) Myciretin, quercetin and kaempferol contents in teas commercialized in Brazil. Food Sci Technol 26:380–385. https://doi.org/10.1590/S0101-20612006000200021
28. Clinical and Laboratory Standards Institute (2018) Methods for dilution antimicrobial susceptibility tests for bacteria that grow aerobically. Approved standard–Seventh edition: M07-A09. 32
29. Pompeu LD, Viana AR, Fernandes LS, Da Silva WL (2023) Evaluation of cytotoxicity, reactive oxygen species and nitrous oxide of nanochitosan from shrimp shell. Int J Biol Macromol 235:123730–123735. https://doi.org/10.1016/j.ijbiomac.2023.123730
30. Vizzotto BS, Dias RS, Iglesias BA, Krause LF, Viana AR, Schuch AP (2020) DNA photocleavage and melanoma cells cytotoxicity induced by a mesotetra-ruthenated porphyrin under visible light irradiation. J Photoch Photobio B 209:111922–111928. https://doi.org/10.1016/j.jphotobiol.2020.111922
31. Mosmann T (1983) Rapid colorimetric assay for cellular growth and survival: application to proliferation and cytotoxicity assays. J Immunol Methods 65:55–63. https://doi.org/10.1016/0022-1759(83)90303-4
32. Sauer H, Wefer K, Vetrugno V, Pocchiari M, Gissel C, Sachinidis A, Hescheler J, Wartenberg M (2003) Regulation of intrinsic prion protein by growth factors and TNFalpha: the role of intracellular reactive oxygen species. Free Radical Bio Med 35:586–594. https://doi.org/10.1016/s0891-5849(03)00360-5
33. Green LC, Wagner DA, Glogowski J, Skipper PL, Wishnok JS, Tannenbaum SR (1982) Analysis of nitrate, nitrite, and nitrate in biological samples. Anal Biochem 126:131–138. https://doi.org/10.1016/0003-2697(82)90118-x
34. Gogate PR, Pandit AB (2004) A review of imperative technologies for wastewater treatment I: oxidation technologies at ambient conditions. Adv Environ Res 8:501–551. https://doi.org/10.1016/S1093-0191(03)00032-7
35. Gaya UI, Abdullah AH (2008) Heterogeneous photocatalytic degradation of organic contaminants over titanium dioxide: a review of fundamentals, progress, and problems. J Photochem Photobiol C 9:1–12. https://doi.org/10.1016/j.jphotochemrev.2007.12.003
36. Alam MA, Subhan N, Rahman MM, Uddin SJ, Reza HM, Sarker SD (2014) Effect of citrus flavonoids, naringin and naringenin, on

metabolic syndrome and their mechanisms of action. Adv Nutr 5:404–417. https://doi.org/10.3945/an.113.005603
37. Malik M, Iqbal MA, Iqbal Y, Malik M, Bakhsh S, Irfan S, Ahmad R, Pham PV (2022) Biosynthesis of silver nanoparticles for biomedical applications: a mini review. Inorg Chem Commun 145:109980–109992. https://doi.org/10.1016/j.inoche.2022.109980
38. Waghchaure RH, Adole VA (2023) Biosynthesis of metal and metal oxide nanoparticles using various parts of plants for antibacterial, antifungal and anticancer activity: a review. J Indian Chem Soc 100:100987–101003. https://doi.org/10.1016/j.jics.2023.100987
39. Rheima AM, Khadom AA, Kadhim MM (2022) Removal of Cibacron Blue P-6B dye from aqueous solution using synthesized anatase titanium dioxide nanoparticles: thermodynamic, kinetic, and theoretical investigations. J Mol Liq 357:119102–119112. https://doi.org/10.1016/j.molliq.2022.119102
40. Reeves P, Ohlhausen R, Sloan D, Pamplin K, Scoggins T, Clark C, Hutchinson B, Green D (1999) Photocatalytic destruction of organic dyes in aqueous TiO2 suspensions using concentrated simulated and natural solar energy. Sol Energy 48:413–420. https://doi.org/10.1016/0038-092X(92)90050-K
41. Vorontsov AV, Tsybulya SV (2018) Influence of nanoparticles size on XRD patterns for small monodisperse nanoparticles of Cu0 and TiO2 anatase. Ind Eng Chem Res 57:2526–2536. https://doi.org/10.1021/acs.iecr.7b04480
42. Chong ZR, Yang SHB, Babu P, Linga P, Li XS (2016) Review of natural gas hydrates as an energy resource: prospects and challenges. Appl Energy 162:1633–1652. https://doi.org/10.1016/j.apenergy.2014.12.061
43. IUPAC (1972) Manual of symbols and terminology. Pure Applied Chemical 31:578
44. McCusker LB, Liebau F, Engelhardt G (2001) Nomenclature of structural and compositional characteristics of ordered microporous and mesoporous materials with inorganic hosts (IUPAC Recommendations 2001). Pure Appl Chem 73:381–394. https://doi.org/10.1351/pac200173020381
45. Nguyen HC, Tran HN, Fu CC, Lu YT, Juang RS (2020) Roles of adsorption and photocatalysis in removing organic pollutants from water by activated carbon–supported titania composites: Kinetic aspects. J Taiwan Inst Chem Eng 109:51–61. https://doi.org/10.1016/j.jtice.2020.02.019
46. Ouyang G, Wang K, Chen XY (2012) TiO2 nanoparticles modified polydimethylsiloxane with fast response time and increased dielectric constant. J Micromech Microeng 22:074002–074011. https://doi.org/10.1088/0960-1317/22/7/074002
47. Da Silva WL, Lasarin ML, Dos Santos JH, Silveira F (2016) Photocatalytic degradation of rhodamine B, paracetamol, and diclofenac sodium by supported titania-based catalysts from petrochemical residue: effect of doping with magnesium. Water Sci Technol 74:2370–2383. https://doi.org/10.2166/wst.2016.362
48. Jassal PS, Kaur D, Prasad R, Singh J (2022) Green synthesis of titanium dioxide nanoparticles: development and applications. J Agr Food Res 10:100361–100374. https://doi.org/10.1016/j.jafr.2022.100361
49. Rokicka-Konieczna P, Wanag A, Sienkiewicz A, Kusiak-Nejman E, Morawski AW (2020) Antibacterial effect of TiO2 nanoparticles modified with APTES. Catal Commun 134:105862–105866. https://doi.org/10.1016/j.catcom.2019.105862
50. Ibhadon AO, Fitzpatrick P (2013) Heterogeneous photocatalysis: recent advances and applications. Catalysts 3:189–218. https://doi.org/10.3390/catal3010189
51. Ali T, Ahmed A, Alam U, Uddin I, Tripathi P, Muneer M (2018) Enhanced photocatalytic and antibacterial activities of Ag-doped TiO2 nanoparticles under visible light. Mater Chem Phys 212:325–335. https://doi.org/10.1016/j.matchemphys.2018.03.052
52. Wolfrum EJ, Huang J, Blake DM, Maness P, Huang Z, Fiest J, Jacoby WA (2002) Photocatalytic oxidation of bacteria, bacterial and fungal spores, and model biofilm components to carbon dioxide on titanium dioxide-coated surfaces. Environ Sci Technol 36:3412–3419. https://doi.org/10.1021/es011423j
53. Sunada K, Watanabe T, Hashimoto K (2003) Bactericidal activity of copper-deposited TiO2 thin film under weak UV light illumination. Environ Sci Technol 37:4785–4789. https://doi.org/10.1021/es034106g
54. Fu G, Vary PS, Lin C (2005) Anatase TiO2 nanocomposites for antimicrobial coatings. J Phys Chem B 109:8889–8898. https://doi.org/10.1021/jp0502196
55. Jin C, Zhu B, Wang X, Lu Q (2008) Cytotoxicity of titanium dioxide nanoparticles in mouse fibroblast cells. Chem Res Toxicol 21:1871–1877. https://doi.org/10.1021/tx800179f
56. Sha B, Gao W, Wang S, Xi F, Lu T (2011) Cytotoxicity of titanium dioxide nanoparticles differs in four liver cells from humans and rat. Composites: Part B-Eng 42:2136–2144. https://doi.org/10.1016/j.compositesb.2011.05.009
57. Tong T, Shereef A, Wu J, Binh CTT, Kelly JJ, Gaillard JF, Gray KA (2013) Effects of material morphology on the phototoxicity of nano-TiO2 to bacteria. Environ Sci Technol 47:12486–12495. https://doi.org/10.1021/es403079h
58. Pantidos N, Horsfall LE (2014) Biological synthesis of metallic nanoparticles by bacteria, fungi and plants. J Nanomed Nanotechnol 5:1000233–1000242. https://doi.org/10.4172/2157-7439.1000233
59. Gholampoor N, Emtiazi G, Emami Z (2015) The influence of microbacterium hominis and bacillus licheniformis extracellular polymers on silver and iron oxide nanoparticles production; green synthesis and mechanism of bacterial nano production. J Nanomater Mol Nanotechnol 4:1–25. https://doi.org/10.4172/2324-8777.1000160
60. Canaparo R, Foglietta F, Limongi T, Serpe L (2021) Biomedical applications of reative oxygen species generation by metal nanoparticles. Materials 14:53–66. https://doi.org/10.3390/ma14010053
61. Fu L, Hamzeh M, Dodard S, Zhao YH, Sunahara GI (2015) Effects of TiO2 nanoparticles on ROS production and growth inhibition using freshwater green algae pre-exposed to UV irradiation. Environ Toxicol Pharmacol 39:1074–1080. https://doi.org/10.1016/j.etap.2015.03.015
62. Yang C, Jiang L, Zhang H, Shimoda LA, DeBerardinis RJ, Semenza G (2014) Chapter Twenty-Two - Analysis of Hypoxia-Induced Metabolic Reprogramming. Meth Enzymol 542:425–455. https://doi.org/10.1016/B978-0-12-416618-9.00022-4
63. Deshpande MS, Kumbhar AA, Kumbhar AS, Kumbhakar M, Pal H, Sonawane UB, Joshi RR (2009) Ruthenium(II) Complexes of bipyridine-glycoluril and their interactions with DNA. Bioconjugate Chem 20:447–459. https://doi.org/10.1021/bc800298t
64. Vasantharaj S, Sathiyavimal S, Senthilkumar P, LewisOscar F, Pugazhendhi A (2019) Green synthesis of iron oxide nanoparticles using leaf extract of Ruellia tuberosa: Antimicrobial properties and their applications in photocatalytic degradation. J Photochem Photobiol B: Biol 192:74–82. https://doi.org/10.1016/j.jphotobiol.2018.12.025
65. Mondal P, Anweshan A, Purkait MK (2020) Green synthesis and environmental application of iron-based nanomaterials and nanocomposite: a review. Chemosphere 259:127509–127535. https://doi.org/10.1016/j.chemosphere.2020.127509
66. Bryan NS, Grusham MB (2007) Methods to detect nitric oxide and its metabolites in biological samples. Free Radic Biol Med 43:645–657. https://doi.org/10.1016/j.freeradbiomed.2007.04.026
67. Brizzolari A, Cas MD, Cialoni D, Marroni A, Morano C, Samaja M, Paroni R, Rubino FM (2021) High-throughput Griess assay of

nitrite and nitrate in plasma and red blood cells for human physiology studies under extreme conditions. Molecules 26:4569–4588. https://doi.org/10.3390/molecules26154569
68. Yuan L, Zhang J, Wu X, Li N, Liu H, He L (2021) The determination of nitrite content in market sausages. IOP Conf. Ser.: Earth Environ. Sci 631:012036–012041. https://doi.org/10.1088/1755-1315/631/1/012036
69. Wei L, Shifu C, Wei Z, Sujuan Z (2009) Titanium dioxide mediated photocatalytic degradation of methamidophos in aqueous phase. J Hazard Mater 164:154–160. https://doi.org/10.1016/j.jhazmat.2008.07.140
70. Pardeshi SK, Patil AB (2009) Effect of morphology and crystallite size on solar photocatalytic activity of zinc oxide synthesized by solution free mechanochemical method. J Mol Catal A Chem 308:32–40. https://doi.org/10.1016/j.molcata.2009.03.023
71. Qamar M, Muneer M (2009) A comparative photocatalytic activity of titanium dioxide and zinc oxide by investigating the degradation of vanillin. Desalination 249:535–540. https://doi.org/10.1016/j.desal.2009.01.022
72. Guettai N, Amar HA (2005) Photocatalytic oxidation of methyl orange in presence of titanium dioxide in aqueous suspension. Part I: parametric study. Desalination 185:427–437. https://doi.org/10.1016/j.desal.2005.04.048
73. Rodrigues MHM, Dos Santos LM, Gonçalves RF, Santos MRC, Gurgel MFC, Godinho MJ (2018) Study kinetic of degradation of blue methylene using catalysts of índium-doped ceria. J Eng Exact Sci 4:28–34. https://doi.org/10.18540/jcecvl4iss1pp0028-0034
74. Inagaki CS, Reis AEDS, Oliveira NM, Paschoal V, Mazali IO, Alfaya AA (2015) Use of SiO2/TiO2 nanostructured composite in the photodegradation of textile dyes with natural sunlight. Quim Nova 38:1037–1043. https://doi.org/10.5935/0100-4042.20150105
75. Chatterjee D, Dasgupta S (2005) Visible light induced photocatalytic degradation of organic pollutants. J Photochem Photobiol C: Photochem Rev 6:186–205. https://doi.org/10.1016/j.jphotochemrev.2005.09.001
76. Ahmad KS, Jaffri SB (2018) Phytosynthetic Ag doped ZnO nanoparticles: semiconducting green remediators. Open Chem J 16:556–570. https://doi.org/10.1515/chem-2018-0060
77. Mishra G, Mukhopadhyay M (2019) TiO2 decorated functionalized halloysite nanotubes (TiO2@HNTs) and photocatalytic PVC membranes synthesis, characterization and its application in water treatment. Sci Rep 9:4345–4361. https://doi.org/10.1038/s41598-019-40775-4
78. Yu C, Tang J, Li F, Chen Y (2021) Green synthesized nanosilver-biochar photocatalyst for persulfate activation under visible-light illumination. Chemosphere 284:131237–131248. https://doi.org/10.1016/j.chemosphere.2021.131237
79. Ashfaq M, Talreja N, Chauhan D, Rodríguez CA, Mera AC, Mangalaraja RV (2021) A novel bimetallic (Fe/Bi)-povidone-iodine micro-flowers composite for photocatalytic and antibacterial applications. J Photochem Photobiol B Biol 219:112204–112214. https://doi.org/10.1016/j.jphotobiol.2021.112204
80. Puga F, Navío JA, Hidalgo MC (2021) Enhanced UV and visible light photocatalytic properties of synthesized AgBr/SnO2 composites. Sep Purif Technol 257:117948–117960. https://doi.org/10.1016/j.seppur.2020.117948